Journal of Applied Mathematics and Physics, 2026, 14(9), 3529-3550
https://www.scirp.org/journal/jamp
ISSN Online: 2327-4379
ISSN Print: 2327-4352

Domain Walls with Deceleration Parameter in $f\left(R, L_m, T\right)$ Theory

Sachin Pralhadrao Hatkar[1], Gajanan Dattarao Karhale[2*], Dnyaneshwar Pralhad Tadas[3], Shivdas Devmanrao Katore[4]

[1]Department of Mathematics, A.E.S. Arts, Commerce and Science College, Hingoli, India
[2]Department of Mathematics, Shankarrao Patil Mahavidyalaya, Bhoom, India
[3]Department of Mathematics, Toshniwal Arts, Commerce and Science College, Sengaon, India
[4]Department of Mathematics, Sant Gadge Baba Amravati University, Amravati, India
Email: *gajanankarhale4949@gmail.com

How to cite this paper: Hatkar, S.P., Karhale, G.D., Tadas, D.P. and Katore, S.D. (2026) Domain Walls with Deceleration Parameter in $f\left(R, L_m, T\right)$ Theory. *Journal of Applied Mathematics and Physics*, **14**, 3529-3550.
https://doi.org/10.4236/jamp.2026.149176

Received: July 31, 2026
Accepted: September 15, 2026
Published: September 18, 2026

Abstract

In this paper, we studied the Friedmann-Robertson-Walker (FRW) space-time with domain walls in the framework of $f\left(R, L_m, T\right)$ theory of gravitation. Field equation of $f\left(R, L_m, T\right)$ are solved by using two model of $f\left(R, L_m, T\right)$ *i.e.* $f\left(R, L_m, T\right) = R - \mu L_m T - \alpha$, $f\left(R, L_m, T\right) = R + \zeta L_m + lT - \beta$ and special form of deceleration parameter with the relation $\rho_{eff} = \omega p_{eff}$. It is observed that the universe is accelerated and expanding.

Keywords

The Domain Wall, FRW, $f\left(R, L_m, T\right)$ Gravity

1. Introduction

The investigation of alternative theories of gravity, particularly those involving a non-minimal coupling between matter and geometry, has gained significant attention due to certain limitations of the standard ΛCDM cosmological model. Although the ΛCDM model is remarkably successful in explaining a wide range of cosmological observations, including Type Ia supernova measurements [1] [2], observations from the Planck mission [3], and data from the Sloan Digital Sky Survey (SDSS) [4], which collectively indicate that the universe is currently undergoing an accelerated phase of expansion, several theoretical challenges remain unresolved. Within the framework of General Relativity (GR), the observed late-time cosmic acceleration cannot be explained solely by ordinary matter and radiation, thereby necessitating the introduction of an exotic component with sufficiently negative pressure [5]. This situation has motivated researchers to pursue two principal approaches: the development of modified theories of gravity and the construction of alternative gravitational frameworks beyond GR.

A notable milestone in cosmology was Einstein's introduction of the cosmological constant Λ into his field equations [6]. This concept later became a fundamental component of the ΛCDM model, where the cosmological constant acts as dark energy while cold dark matter accounts for the formation and evolution of large-scale structures [7]. Despite its outstanding agreement with observational data, the ΛCDM paradigm is confronted with significant theoretical issues, most notably the cosmological constant problem, which arises from the enormous discrepancy between the observed value of Λ and the value predicted by quantum field theories [8] [9]. These challenges have motivated the exploration of alternative gravitational theories that may provide a more comprehensive description of the universe and its accelerated expansion.

To explore the phenomenon of cosmic acceleration, various alternative models have been proposed, including numerous dark energy theories and modifications to GR [10] [11]. Some studies employ thermodynamic approaches to investigate the evolution of the deceleration parameter [12], while others examine the influence of additional barotropic fluids [13]. Furthermore, cosmographic techniques [13], holographic dark energy models [14], and analyses based on curvature eigenvalues [15] have been developed. Intermediate-redshift calibration methods have also provided valuable tools for examining cosmic correlations [16]. One of the earliest and most extensively studied modifications of General Relativity is the $f(R)$ gravity theory, in which the Einstein-Hilbert action is generalized by replacing the Ricci scalar R with an arbitrary function $f(R)$. This framework offers a purely geometric explanation for the late-time accelerated expansion of the Universe without invoking dark energy. The theory reduces to General Relativity for the particular choice $f(R)=R$, whereas the inclusion of higher-order curvature terms enables the investigation of more complex cosmological dynamics [17].

More recently, gravitational theories involving matter geometry coupling have attracted considerable attention. In these models, modifications to gravity arise from direct interactions between matter and spacetime geometry. In particular, the $f(R,T)$ gravity theory, where T denotes the trace of the energy momentum tensor, provides a natural extension of $f(R)$ gravity and has been widely applied in cosmological studies. The modified gravity theories $f(R,T)$ [18] and $f(R,L_m)$ [19] have attracted considerable attention in recent years. The $f(R,T)$ framework incorporates both the Ricci scalar R and the trace of the energy momentum tensor T, introducing a coupling that permits the non-conservation of the energy momentum tensor. This feature has significant implications for cosmological dynamics, particularly in the presence of imperfect fluids [18]. On the other hand the $f(R,L_m)$ theory extends the gravitational Lagrangian by allowing an explicit dependence on the matter Lagrangian density L_m in addition to R, thereby enabling direct interactions between matter and geometry [19]. Such interactions may generate extra forces acting on massive particles and provide a useful framework for modeling dark sector phenomena.

Furthermore, the hybrid metric-Palatini gravity formalism offers a unified theoretical framework capable of addressing both cosmological and astrophysical challenges while remaining consistent with local gravitational tests. This approach has been proposed as a promising avenue for explaining the nature of dark energy and dark matter [20]. These modified theories of gravity have been extensively studied in various cosmological and astrophysical contexts. Recently, Haghani and Harko [21] introduced an extended class of modified gravity theories characterized by a non-minimal coupling between matter and geometry, known as $f(R, L_m, T)$ gravity. Zubair *et al.* [22] studied Stellar configurations in $f(R, L_m, T)$ gravity probing anisotropy and stability via minimal geometric deformation. Koussour *et al.* [23] investigated Late time acceleration in extended and unified $f(R, L_m, T)$ gravity with observational data. Kiroriwal *et al.* [24] investigated wormhole solutions in $f(R, L_m, T)$ gravity using a density gradient-dependent equation of state. Naseer *et al.* [25] studied cosmological models in $f(R, L_m, T)$ gravity using the gravitational decoupling approach and studied different phases of cosmic evolution. Mishra *et al.* [26] studied comparative study on neutron star structure in linear and non-linear matter-curvature coupling in $f(R, L_m, T)$ gravity using equation of states. In addition, several wormhole solutions have been obtained in the context of $f(R, L_m, T)$ gravity [27] [28].

Understanding the exact physical conditions that existed during the early evolution of the universe remains one of the major challenges in cosmology. It is widely believed that topological defects were produced during phase transitions in the early universe because of the spontaneous breaking of discrete symmetries. Among these defects, domain walls, cosmic strings, and monopoles are the most important stable structures. In recent years, domain wall cosmological models have attracted significant attention due to their unique properties and interesting gravitational effects, making them an active area of research. Various studies have examined domain walls under different theoretical frameworks. Katore *et al.* [29]-[31] studied domain walls in various cosmological scenarios. Vilenikin [32], Isper and Sikivie [33], Reddy *et al.* [34], Mukherjee [35] are some of the authors who have studied several aspects of domain walls in various context. Pradhan *et al.* [36] discussed solutions for inhomogeneous bulk viscosity with domain walls in the Lyra geometry in the plane symmetric space-time. Reddy *et al.* [37] have investigated a locally rotationally symmetric Bianchi type II space-time in the framework of the modified theory of gravitation.

The motivation for the present study is to study the cosmic evolution of domain walls in the framework of $f(R, L_m, T)$ gravity for Friedman-Robertson-Walker (FRW) metric. This theory provides a generalized description of gravity through the coupling of geometry with matter. By incorporating a deceleration parameter, we aim to study the expansion history of the universe and the behavior of domain wall energy density. By using this study we can examine whether the model can describe the transition from decelerated to accelerated expansion. We derive the solution of field equation using deceleration parameter, $p_{eff} = \omega\rho_{eff}$ and two model of $f(R, L_m, T)$ theory. This paper is organized as follows, Section 2 deals with metric and field equation. In Section 3 and Section 4, we obtained solution of field equations. Section 5 deals conclusion of this paper.

2. Metric and Field Equation

The $f(R, L_m, T)$ gravity theory, proposed by Haghani and Harko [21], is a generalized version of the $f(R, T)$ [18] and $f(R, L_m)$ [19] gravity models. In this theory, the gravitational Lagrangian is taken as an arbitrary function of the Ricci scalar R, the trace T of the energy-momentum tensor, and the matter Lagrangian L_m. Therefore, the action in $f(R, L_m, T)$ gravity depends on both the geometrical and matter components of the universe.

Action of $f(R, L_m, T)$ theory is given by

$$S = \frac{1}{16\pi}\int f(R, L_m, T)\sqrt{-g}\,\mathrm{d}^4x + \int L_m\sqrt{-g}\,\mathrm{d}^4x, \tag{1}$$

where g is the determinant of the metric tensor $g_{\mu\nu}$.

Now, after varying the action (1) with respect to the metric tensor $g_{\mu\nu}$, we obtains the following field equations in $f(R, L_m, T)$ gravity

$$\begin{aligned} &f_R R_{\mu\nu} - \frac{1}{2}\left[f - \left(f_{L_m} + 2f_T\right)L_m\right]g_{\mu\nu} + \left(g_{\mu\nu}\Box - \nabla_\mu\nabla_\nu\right)f_R \\ &= \left[8\pi + \frac{1}{2}\left(f_{L_m} + 2f_T\right)\right]T_{\mu\nu} + f_T\tau_{\mu\nu} \end{aligned} \tag{2}$$

Here, notations $\Box = \frac{1}{\sqrt{-g}}\partial_\alpha\left(\sqrt{-g}g^{\alpha\beta}\partial_\beta\right)$, $f_R = \frac{\partial f}{\partial R}$, $f_{L_m} = \frac{\partial f}{\partial L_m}$, $f_T = \frac{\partial f}{\partial T}$, $R_{\mu\nu}$ is the Ricci tensor, ∇_μ the covariant derivative with respect to the symmetric connection associated to $g_{\mu\nu}$, and new tensor $\tau_{\mu\nu}$ is defined as [21]

$$\tau_{\mu\nu} = 2g^{\mu\nu}\frac{\partial^2 L_m}{\partial g^{\mu\nu}\partial g^{\alpha\beta}}. \tag{3}$$

For a perfect fluid matter Lagrangian L_m defined as $L_m = -\rho_{eff}$ where ρ_{eff} is the energy density and the additional term $\tau_{\mu\nu}$ turns out to be zero [21]. Now we get modified field equation from Equation (2)

$$\left(R_{\mu\nu} + g_{\mu\nu}\Box - \nabla_\mu\nabla_\nu\right)f_R - \frac{1}{2}fg_{\mu\nu} = 8\pi T_{\mu\nu} + \frac{1}{2}\left(f_{L_m} + 2f_T\right)\left(T_{\mu\nu} - L_m g_{\mu\nu}\right) \tag{4}$$

We consider the Friedmann-Robertson-Walker (FRW) [29] cosmological model in the following form;

$$\mathrm{d}s^2 = \mathrm{d}t^2 - a^2\left(\frac{\mathrm{d}r_1^2}{1 - kr_1^2} + r_1^2\left(\mathrm{d}\theta^2 + \sin^2\theta\,\mathrm{d}\phi\right)\right) \tag{5}$$

In FRW space time, the angles $0 \le \theta \le 2\pi$ and $0 \le \phi \le 2\pi$ are the usual azimuthal and polar angles of spherical coordinates. The k represents the curvature of the space. The curvature of space has three different values. When $k = 1$

the radius is finite and the universe is closed. When $k = 0$, the universe is flat and when $k = -1$ the radius is infinite or imaginary corresponding to open universe [38].

The Ricci scalar R associated with the line element (12) can be derived as follows

$$R = -6\left[\frac{k}{a^2} + \left(\frac{\dot{a}}{a}\right)^2 + \frac{\ddot{a}}{a}\right] \tag{6}$$

where a is scale factor.

The energy momentum tensor of domain walls [29] is given as:

$$T_{ij} = \rho_{eff}\left(g_{ij} + \mu_i \mu_j\right) + p_{eff}\mu_i\mu_j \tag{7}$$

here ρ_{eff}, p_{eff} denotes energy density and pressure of domain wall respectively, and μ_i is the four velocity vector with components $(0,0,0,1)$ in the same direction with $\mu_i \mu^i = -1$. Based on the default model of particle physics, it is assumed that when the hot early universe cooled and expanded, the field would have settled to single values during extended regions. The boundaries of those different regions would be the domain walls. The energy momentum tensor T_{ij} of domain walls include normal matter ρ_m and pressure p_m as well as tension σ_d with the relation

$$p_{eff} = p_m - \sigma_d \tag{8}$$

$$\rho_{eff} = \rho_m + \sigma_d \tag{9}$$

satisfying

$$p_m = (\gamma - 1)\rho_m \tag{10}$$

where, $1 \le \gamma \le 2$.

The field equation for line element (5) using Equations (1) and (7)

$$\begin{aligned} & f_R\left[\frac{2k}{a^2} + 2\left(\frac{\dot{a}}{a}\right)^2 + \frac{\ddot{a}}{a}\right] - \frac{3\dot{a}}{a}\dot{f}_R - \ddot{f}_R + \frac{f}{2} \\ & = \frac{1}{2}\left(f_{L_m} + 2f_T\right)L_m - \left[8\pi + \frac{1}{2}\left(f_{L_m} + 2f_T\right)\right]\rho_{eff} \end{aligned} \tag{11}$$

$$\frac{3\ddot{a}}{a}f_R - \frac{3\dot{a}}{a}\dot{f}_R + \frac{f}{2} = \frac{1}{2}\left(f_{L_m} + 2f_T\right)L_m + \left[8\pi + \frac{1}{2}\left(f_{L_m} + 2f_T\right)\right]p_{eff} \tag{12}$$

where overdot (.) represent differentiation with respect to cosmic time t. We obtained two Equations (11) and (12) with three unknown a, ρ_{eff} and p_{eff}.

To obtain exact solution of field equation we consider two model of $f(R, L_m, T)$ theory, relation $p_{eff} = \omega\rho_{eff}$ and and deceleration parameter (DP) *q*.

Relation of equation of state is given as

$$p_{eff} = \omega\rho_{eff}, \tag{13}$$

The Hubble parameter is taken as [39]

$$H(t)=\frac{n}{t\left(m-t^{r}\right)}, \tag{14}$$

where m, n, and r are model parameters. This parametrization generates different cosmological models depending on the value of r. Using the relation between the Hubble parameter and the deceleration parameter,

$$q=1-\frac{\dot{H}}{H^{2}}. \tag{15}$$

The corresponding deceleration parameter is obtained as

$$q=\frac{-\ddot{a}a}{\dot{a}^{2}}=-1+\frac{m}{n}-\frac{r+1}{n}t^{r}. \tag{16}$$

Thus, for different values of r, the model get different form of the deceleration parameter. Specifically, ($r=0$): Constant Deceleration Parameter (CDP) model, $r=1$ Linearly Varying Deceleration Parameter (LVDP) model, $r=2$ Quadratically Varying Deceleration Parameter (QVDP) model, $r=3$ Cubically Varying Deceleration Parameter (CVDP) model, $r=4$ Quartically Varying Deceleration Parameter (QUADP) model, $r=5$ Quintically Varying Deceleration Parameter (QUIDP) model.

Using Equation (16) scale factor $a(t)$ is obtained as

$$a(t)=c\left(\frac{t^{r}}{m-t^{r}}\right)^{\frac{n}{rm}}, \tag{17}$$

where c is the constant.

The relation of red shift and scale factor is defined as $1+z=\frac{a_0}{a}$, where a_0 is the present value of the scale factor.

The deceleration parameter and Hubble parameter in term of red shift obtained as follows

$$q(z)=-1+\lambda-\frac{(r+1)\lambda}{1+\left[\eta(1+z)\right]^{r\lambda}} \tag{18}$$

and

$$H(z)=\frac{H_0\left\{1+\left[\eta(1+z)\right]^{r\lambda}\right\}^{\left(\frac{r+1}{r}\right)}}{\left(1+\eta^{r\lambda}\right)^{\left(\frac{r+1}{r}\right)}(1+z)^{r\lambda}}, \tag{19}$$

where η and λ are new parameter regarding to m and n.

Figure 1 shows the variation of the deceleration parameter q versus redshift z for different values of the parameter r. It shows that the value of q increases as redshift increases. For different values of r the curve of DP have similar behavior. The negative values of DP represent the accelerated expansion of the universe, while the positive values indicate a decelerating phase. At high value of redshift DP is positive for $r=2$, $r=3$ and $r=4$, as value of redshift decreases, DP is negative. It shows that in past universe is decelerated and in future it is accelerated for different values of the parameter r.

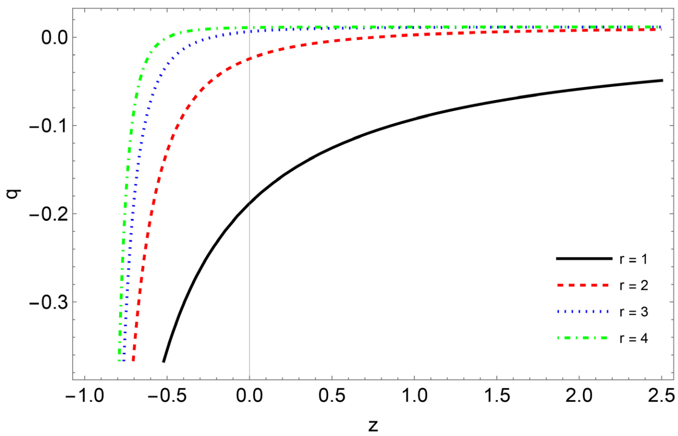

Figure 1. Plot of Deceleration Parameter q vs. red shift z for $\eta = 8.9$, $\lambda = 1.011$.

3. Model I

In this model we consider the $f(R, L_m, T)$ model as [21]

$$f(R, L_m, T) = R - \mu L_m T - \alpha, \tag{20}$$

where μ and α are arbitrary constants and $L_m = -\rho_{eff}$ where ρ_{eff} is energy density.

Using Equations (6), (12), (13) (17) and (20) ρ_{eff} is obtained as

$$\rho_{eff} = \frac{8\pi\omega + \sqrt{(8\pi\omega)^2 + 4l_1\left\{\frac{\alpha}{2} + 3k(1+z)^2 + \frac{3H_0^2\left\{1+\left[\eta(1+z)\right]^{r\lambda}\right\}^{2\left(\frac{r+1}{r}\right)}}{\delta^2(1+z)^{2r\lambda}}\right\}}}{l_1}, \tag{21}$$

where $l_1 = \mu + \frac{1}{2}\mu\omega - \frac{1}{2}\omega^2$, $\delta = \left(1+\eta^{r\lambda}\right)^{\frac{r+1}{r}}$.

Figure 2 and **Figure 3** shows that the variation of the energy density ρ_{eff} versus redshift z for different values of curvature parameters $k=1$, $k=-1$, $k=0$ and model parameters $r=1$, $r=2$, $r=3$, $r=4$. These graphs of **Figures 2(a)-(f)** and **Figures 3(a)-(f)** represents two different trajectories for $\omega = 1$ and $\omega = -1$ while the remaining parameters fixed at $\mu = 5.9$, $\lambda = 1.011$, $\eta = 8.9$, $\alpha = 1.9$, and $H_0 = 71$. It shows that energy density is high at high value of redshift and it is tends to zero as $z \to -1$, indicating that at early time of the universe energy density was very high and at late time of the universe it tends to zero. Furthermore, the model shows larger values of ρ_{eff} for the dark-energy-dominated case $\omega = -1$ than for the stiff-fluid case $\omega = 1$ in the range of the redshift. **Figure 2** and **Figure 3** shows that as value of parameters $r=1$, $r=2$, $r=3$, $r=4$ increases then energy density is also increases. While as curvature parameter k changes from 1 to −1 or 0 produces only minor quantitative differences, while the overall changes of the all graphs are same. This indicates that the parameter r has a stronger influence on the evolution of the energy density than the curvature parameter k.

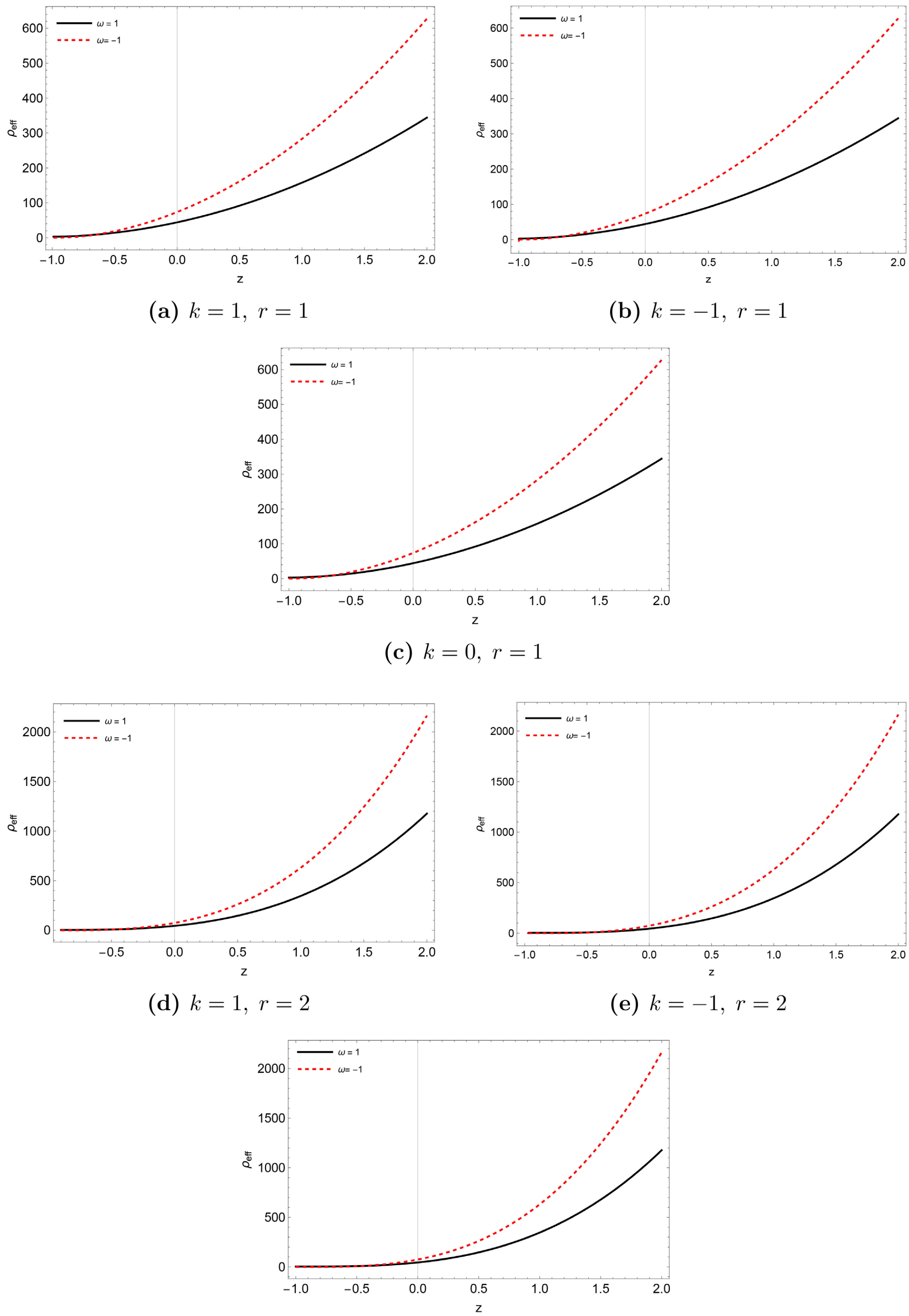

(a) $k = 1,\ r = 1$ (b) $k = -1,\ r = 1$

(c) $k = 0,\ r = 1$

(d) $k = 1,\ r = 2$ (e) $k = -1,\ r = 2$

(f) $k = 0,\ r = 2$

Figure 2. Graphical representation of the Energy density ρ_{eff} for different values of k and r. The parameters are fixed at $\mu = 5.9$, $\lambda = 1.011$, $\eta = 8.9$, $\alpha = 1.9$ and $H_0 = 71$.

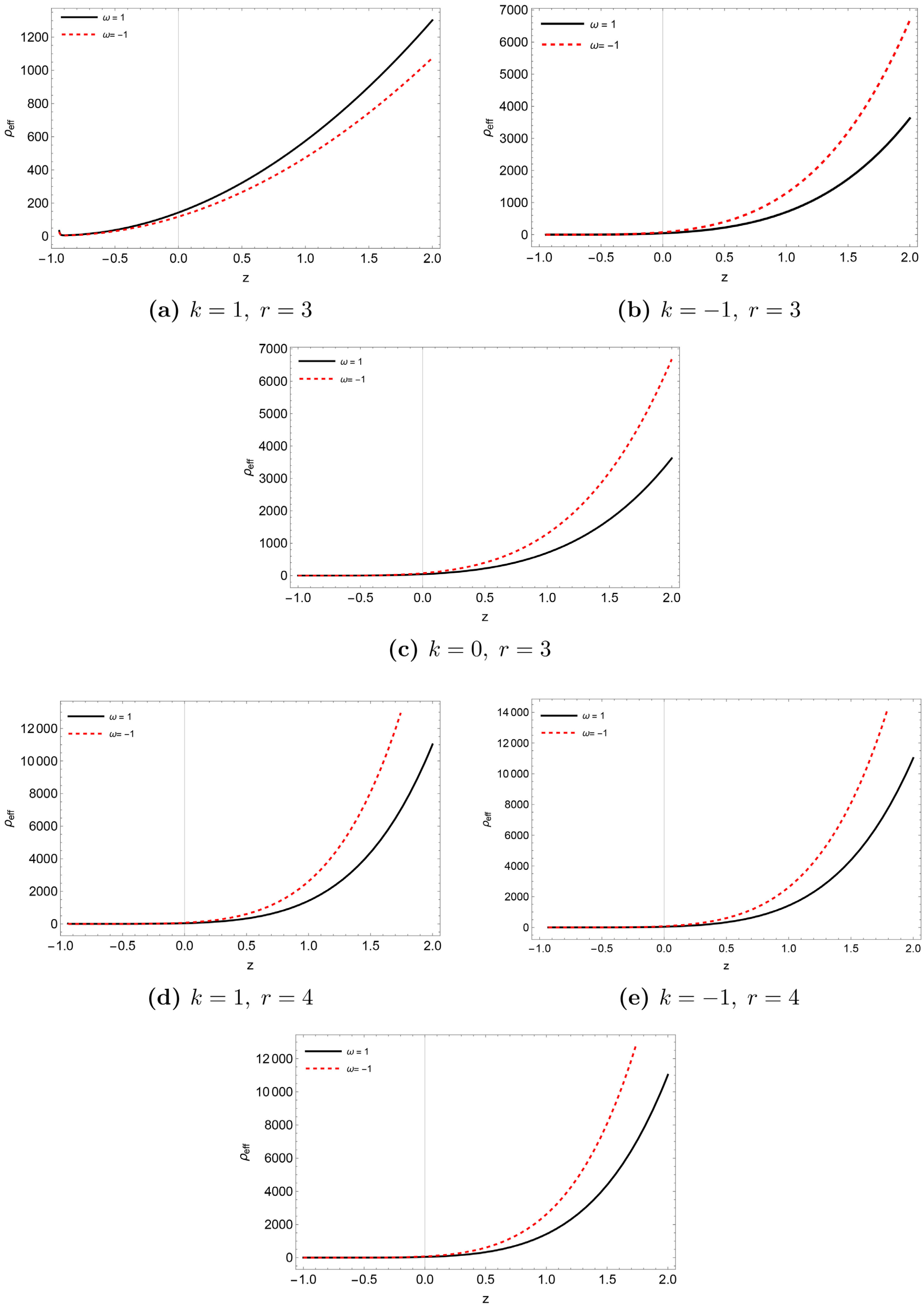

(a) $k=1,\ r=3$ (b) $k=-1,\ r=3$

(c) $k=0,\ r=3$

(d) $k=1,\ r=4$ (e) $k=-1,\ r=4$

(f) $k=0,\ r=4$

Figure 3. Graphical representation of the Energy density ρ_{eff} for different values of k and r. The parameters are fixed at $\mu=5.9$, $\lambda=1.011$, $\eta=8.9$, $\alpha=1.9$ and $H_0=71$.

Overall, the obtained behavior is physically consistent with the standard cosmological picture, where the matter-energy content of the universe becomes increasingly concentrated at higher redshifts, and the dark-energy equation of state yields comparatively higher energy densities within the present model.

Using Equations (8), (9), (10), (11), (20) and (21) energy density of normal matter ρ_m is obtained as

$$\rho_m = \frac{4\left\{k(1+z)^2\delta^2(1+z)^{2r\lambda} + 2H_0(l_2)^{\frac{1}{r}} r\lambda(1+z)^{r\lambda-1}\delta\left[\frac{\left[\eta(1+z)\right]^{r\lambda}-r}{r}\right] + 3H_0^2(l_2)^{2\left(\frac{r+1}{r}\right)} + \frac{\alpha}{2}\right\}l_1}{\mu\gamma\delta^2(1+z)^{2r\lambda}\left[8\pi\omega + \sqrt{(8\pi\omega)^2 + 4l_1\left\{\frac{\alpha}{2} + 3k(1+z)^2 + \frac{3H_0^2\left\{1+\left[\eta(1+z)\right]^{r\lambda}\right\}^{2\left(\frac{r+1}{r}\right)}}{\delta^2(1+z)^{2r\lambda}}\right\}}\right]} - \frac{16\pi}{\mu\gamma}, \tag{22}$$

where $l_2 = \left[\eta(1+z)\right]^{r\lambda} + 1$.

Also, the tension of domain walls σ_d is found to be as

$$\sigma_d = \frac{8\pi\omega + \sqrt{(8\pi\omega)^2 + 4l_1\left\{\frac{\alpha}{2} + 3k(1+z)^2 + \frac{3H_0^2\left\{1+\left[\eta(1+z)\right]^{r\lambda}\right\}^{2\left(\frac{r+1}{r}\right)}}{\delta^2(1+z)^{2r\lambda}}\right\}}}{l_1} - \frac{4\left\{k(1+z)^2\delta^2(1+z)^{2r\lambda} + 2H_0(l_2)^{\frac{1}{r}} r\lambda(1+z)^{r\lambda-1}\delta\left[\frac{\left[\eta(1+z)\right]^{r\lambda}-r}{r}\right] + 3H_0^2(l_2)^{2\left(\frac{r+1}{r}\right)} + \frac{\alpha}{2}\right\}l_1}{\mu\gamma\delta^2(1+z)^{2r\lambda}\left[8\pi\omega + \sqrt{(8\pi\omega)^2 + 4l_1\left\{\frac{\alpha}{2} + 3k(1+z)^2 + \frac{3H_0^2\left\{1+\left[\eta(1+z)\right]^{r\lambda}\right\}^{2\left(\frac{r+1}{r}\right)}}{\delta^2(1+z)^{2r\lambda}}\right\}}\right]} + \frac{16\pi}{\mu\gamma}. \tag{23}$$

Figure 4 and Figure 5 shows that the variation of the tension of domain walls σ_d versus redshift z for different values of curvature parameters $k=1$, $k=-1$, $k=0$ and model parameters $r=1$, $r=2$, $r=3$, $r=4$. These graphs of Figures 4(a)-(f) and Figures 5(a)-(f) represents two different trajectories for $\omega=1$ and $\omega=-1$ while the remaining parameters fixed at $\mu=5.9$, $\lambda=1.011$, $\eta=8.9$, $\alpha=1.9$, and $H_0=71$, $\gamma=1$. It shows that tension of domain walls is high and positive at high value of redshift, the positive tension indicates that the domain walls possess a large amount of energy. Besides mass, pressure and tension also contribute to the gravitational field. As value of redshift decrease, the trajectory of tension of domain walls is decreases and in future it is negative

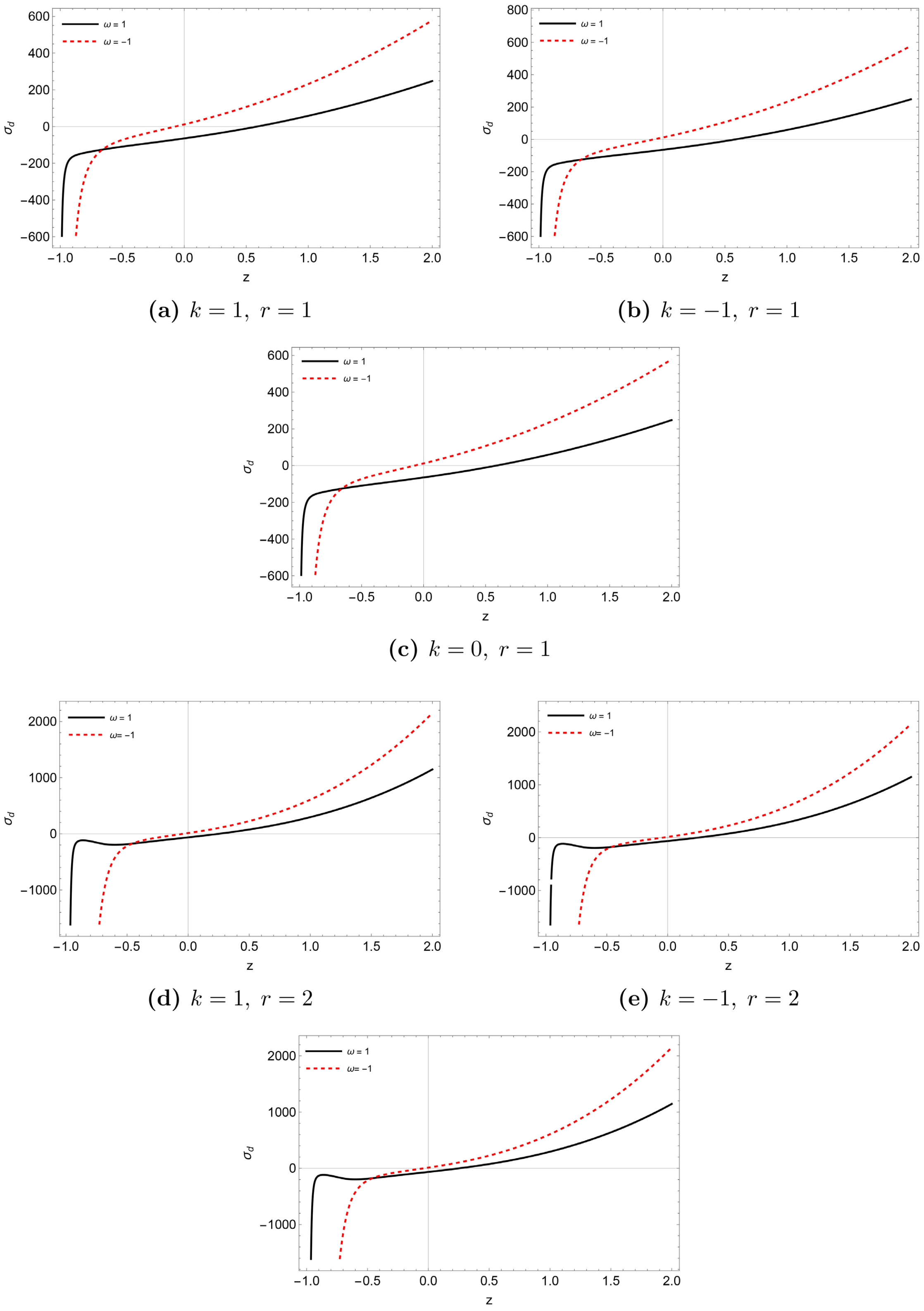

(a) $k = 1,\ r = 1$ **(b)** $k = -1,\ r = 1$

(c) $k = 0,\ r = 1$

(d) $k = 1,\ r = 2$ **(e)** $k = -1,\ r = 2$

(f) $k = 0,\ r = 2$

Figure 4. Graphical representation of the Tension of domain walls σ_d for different values of k and r. The parameters are fixed at $\mu = 5.9$, $\lambda = 1.011$, $\eta = 8.9$, $\alpha = 1.9$, $H_0 = 71$ and $\gamma = 1$.

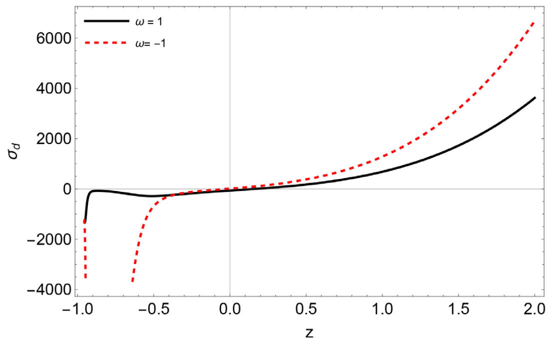

(a) $k = 1, \ r = 3$

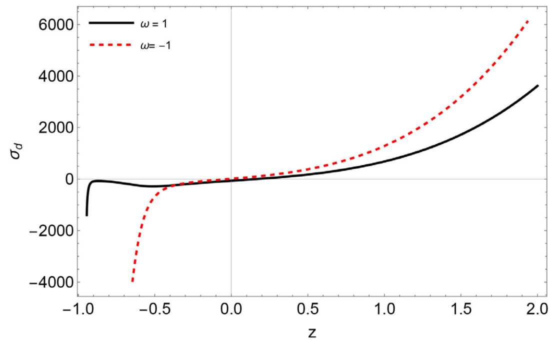

(b) $k = -1, \ r = 3$

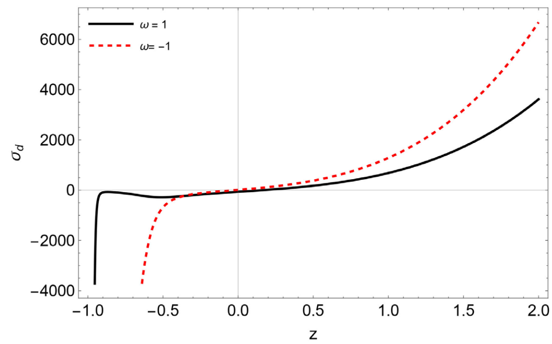

(c) $k = 0, \ r = 3$

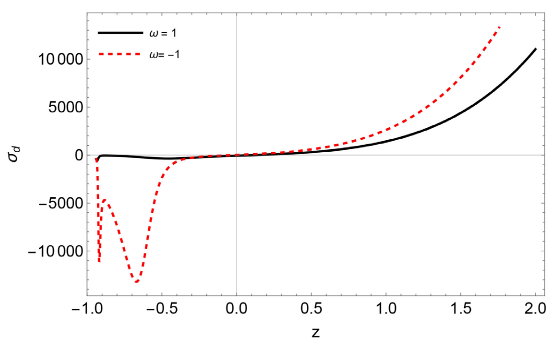

(d) $k = 1, \ r = 4$

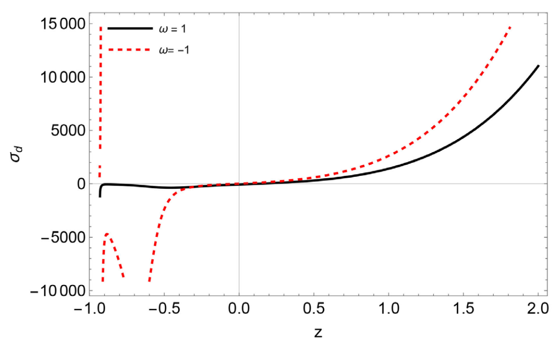

(e) $k = -1, \ r = 4$

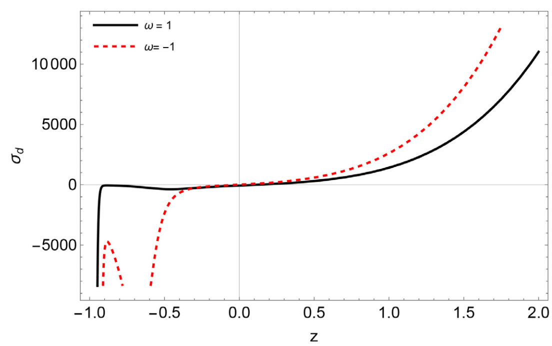

(f) $k = 0, \ r = 4$

Figure 5. Graphical representation of the Tension of domain walls σ_d for different values of k and r. The parameters are fixed at $\mu = 5.9$, $\lambda = 1.011$, $\eta = 8.9$, $\alpha = 1.9$, $H_0 = 71$ and $\gamma = 1$.

for different values of parameter r behaving like a negative pressure. This negative pressure produces a repulsive effect, which supports the accelerated expansion of the universe. These results are consistent with our earlier findings in $f(Q)$ gravity theory [40]. Furthermore, the model shows larger values of σ_d for the dark-energy-dominated case $\omega=-1$ than for the stiff-fluid case $\omega=1$ in the range of the redshift. Figure 4 and Figure 5 shows that as value of parameters $r=1$, $r=2$, $r=3$, $r=4$ increases then tension of domain walls is high. While as curvature parameter k changes from 1 to −1 or 0 produces only minor quantitative differences, while the overall changes of the all graphs are same. This indicates that the parameter r has a stronger influence on the evolution of the tension of domain walls than the curvature parameter k.

4. Model II

In this model we consider $f(R,L_m,T)$ model as [41]

$$f(R,L_m,T)=R+\zeta L_m+lT-\beta, \tag{24}$$

where ζ, l and β are arbitrary constants.

Using Equations (6), (12), (13) (17) and (24) ρ_{eff} is obtained as

$$\rho_{eff}=\frac{\left\{k(1+z)^2\delta^2(1+z)^{2r\lambda}+2H_0(l_2)^{\frac{1}{r}}r\lambda(1+z)^{r\lambda-1}\delta\left[\frac{\left[\eta(1+z)\right]^{r\lambda}-r}{r}\right]+3H_0^2(l_2)^{2\left(\frac{r+1}{r}\right)}+\frac{\beta}{2}\right\}}{\delta^2(1+z)^{2r\lambda}l_3}. \tag{25}$$

where $l_3=8\pi+\frac{\zeta}{2}+\frac{7l}{2}-\frac{l\omega}{2}$

Figure 6 and Figure 7 shows that the variation of the energy density ρ_{eff} versus redshift z for different values of curvature parameters $k=1$, $k=-1$, $k=0$ and model parameters $r=1$, $r=2$, $r=3$, $r=4$. These graphs of Figures 6(a)-(f) and Figures 7(a)-(f) represents two different trajectories for $\omega=1$ and $\omega=-1$ while the remaining parameters fixed at $l=15.1$, $\lambda=1.011$, $\eta=8.9$, $\zeta=1.9$, $\beta=2.5$ and $H_0=71$. It shows that as value of redshift increases, energy density is high as redshift decreases energy density is also decreases and tends to zero as $z\to-1$. At early time of the universe energy density is high and at late time of the energy density is very low.

Furthermore, the model shows larger values of ρ_{eff} for the stiff-fluid case $\omega=1$ than the dark-energy-dominated case $\omega=-1$ in the range of the redshift. Figure 6 and Figure 7 shows that as value of parameters $r=1$, $r=2$, $r=3$, $r=4$ increases then energy density is also increases. While as curvature parameter k changes from 1 to −1 or 0 produces only minor quantitative differences, while the overall changes of the all graphs are same. This indicates that the parameter r has a stronger influence on the evolution of the energy density than the curvature parameter k.

Using Equations (8), (9), (10), (11), (24) and (25) energy density of normal matter ρ_m is obtained as

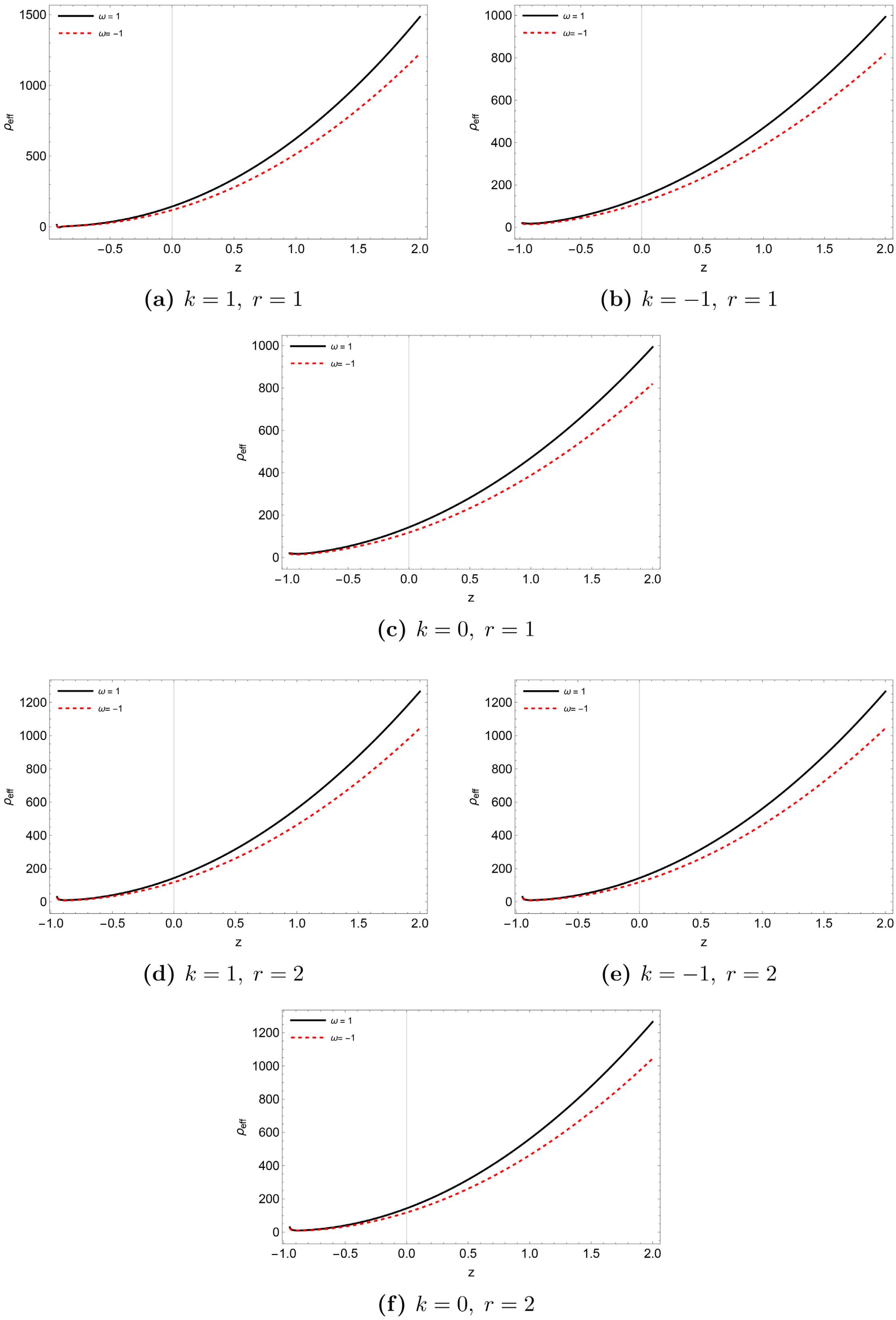

(a) $k=1,\ r=1$ **(b)** $k=-1,\ r=1$

(c) $k=0,\ r=1$

(d) $k=1,\ r=2$ **(e)** $k=-1,\ r=2$

(f) $k=0,\ r=2$

Figure 6. Graphical representation of the Energy density ρ_{eff} for different values of k and r. The parameters are fixed at $l=15.1$, $\lambda=1.011$, $\eta=8.9$, $\zeta=1.9$, $\beta=2.5$ and $H_0=71$.

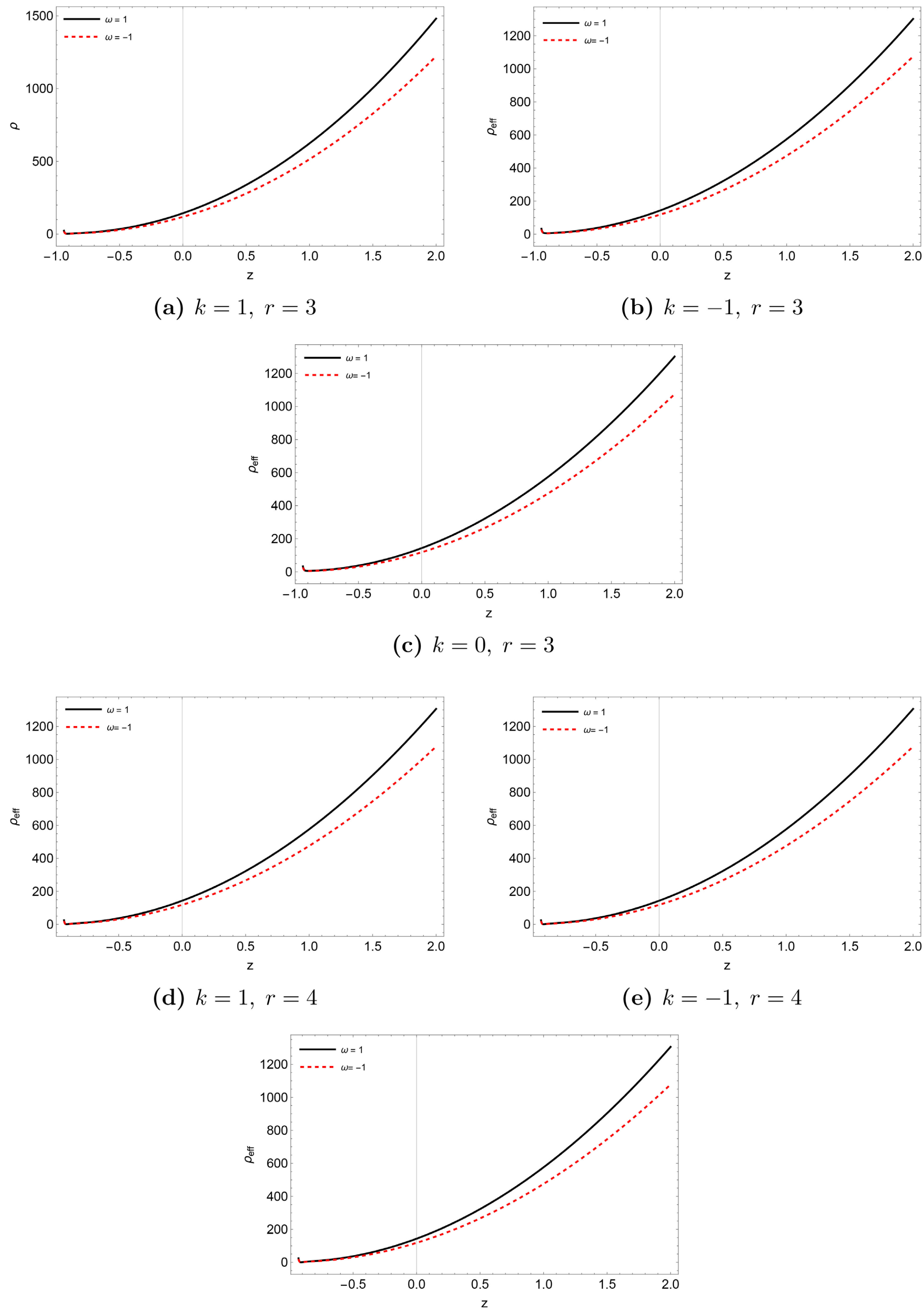

(a) $k=1,\ r=3$

(b) $k=-1,\ r=3$

(c) $k=0,\ r=3$

(d) $k=1,\ r=4$

(e) $k=-1,\ r=4$

(f) $k=0,\ r=4$

Figure 7. Graphical representation of the Energy density ρ_{eff} for different values of k and r. The parameters are fixed at $l=15.1$, $\lambda=1.011$, $\eta=8.9$, $\zeta=1.9$, $\beta=2.5$ and $H_0=71$.

$$\rho_m = \frac{-(3l_3 + l_4)\left\{k(1+z)^2\delta^2(1+z)^{2r\lambda} + H_0^2(l_2)^{2\left(\frac{r+1}{r}\right)}\right\}}{l_3 l_5 \delta^2 (1+z)^{2r\lambda}} - \frac{l_4\left\{2H_0(l_2)^{\frac{1}{r}} r\lambda(1+z)^{r\lambda-1}\delta\left[\frac{[\eta(1+z)]^{r\lambda}-r}{r}\right] + H_0^2(l_2)^{2\left(\frac{r+1}{r}\right)} + \frac{\beta}{2}\right\}}{l_3 l_5 \delta^2 (1+z)^{2r\lambda}}. \tag{26}$$

Furthermore, the tension of domain walls found to be

$$\sigma_d = \frac{(3l_3 + l_4 + l_5)\left\{k(1+z)^2\delta^2(1+z)^{2r\lambda} + H_0^2(l_2)^{2\left(\frac{r+1}{r}\right)}\right\}}{l_3 l_5 \delta^2 (1+z)^{2r\lambda}} + \frac{(l_4 + l_5)\left\{2H_0(l_2)^{\frac{1}{r}} r\lambda(1+z)^{r\lambda-1}\delta\left[\frac{[\eta(1+z)]^{r\lambda}-r}{r}\right] + H_0^2(l_2)^{2\left(\frac{r+1}{r}\right)} + \frac{\beta}{2}\right\}}{l_3 l_5 \delta^2 (1+z)^{2r\lambda}}. \tag{27}$$

where

$$l_4 = \frac{\zeta}{2} - \frac{3l}{2} + \frac{l\omega}{2} + 8\pi\omega,$$

$$l_5 = \left(\frac{\zeta}{2} + l\right)\gamma$$

Figure 8 and Figure 9 shows that the tension of domain walls versus redshift z for various values of curvature parameters $k=1$, $k=-1$, $k=0$ and model parameters $r=1$, $r=2$, $r=3$, $r=4$. These graphs of Figures 8(a)-(f) and Figures 9(a)-(f) represents two different trajectories for $\omega=1$ and $\omega=-1$ while the remaining parameters fixed at $l=15.1$, $\lambda=1.011$, $\eta=8.9$, $\zeta=1.9$, $\beta=2.5$, $H_0=71$, $\gamma=1$. It show that as value of redshift increases, tension of domain walls is high as redshift decreases tension of domain walls is also decreases and tends to zero as $z \to -1$. At early time of the universe tension of domain walls is high and at late time of the universe tension of domain walls is very low and tends to zero. This indicates that domain walls disappear in the far future, which has shown same result by Katore *et al.* [29].

Furthermore, the model shows larger values of σ_d for the stiff-fluid case $\omega=1$ than the dark-energy-dominated case $\omega=-1$ in the range of the redshift. Figure 8 and Figure 9 shows that as value of parameters $r=1$, $r=2$, $r=3$, $r=4$ increases then tension of domain walls is also increases. While curvature parameter k have minor change for $k=1$, $k=-1$ and $k=0$, while the overall changes of the all graphs are same. This indicates that the parameter r has a stronger influence on the evolution of the tension of domain walls than the curvature parameter k.

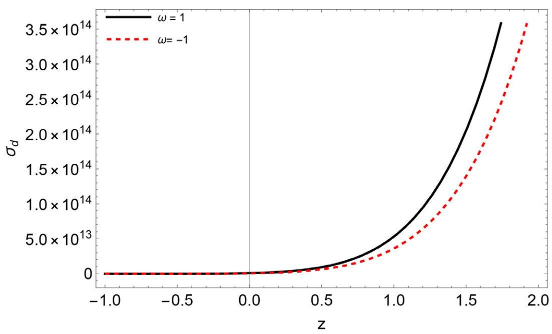

(a) $k = 1,\ r = 1$

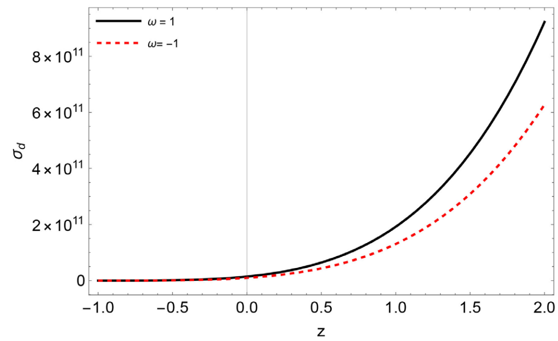

(b) $k = -1,\ r = 1$

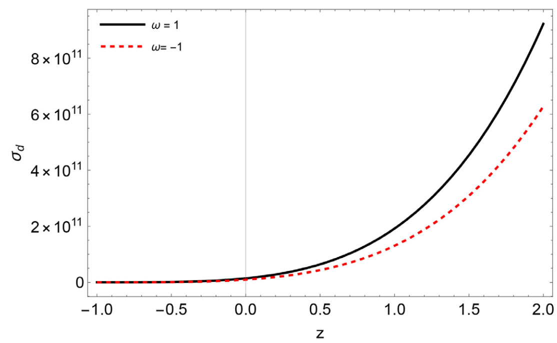

(c) $k = 0,\ r = 1$

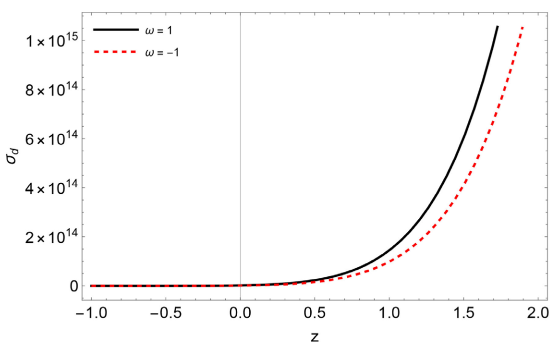

(d) $k = 1,\ r = 2$

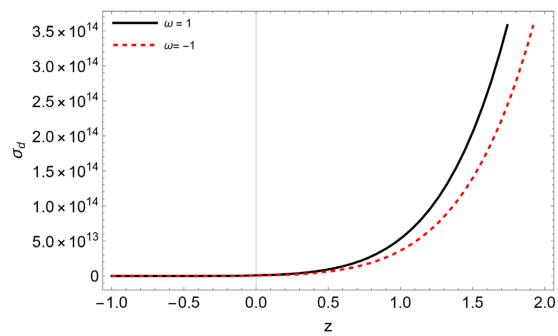

(e) $k = -1,\ r = 2$

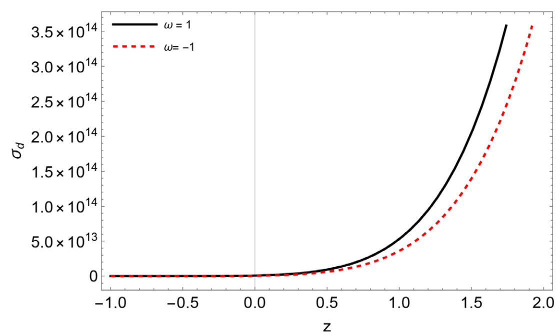

(f) $k = 0,\ r = 2$

Figure 8. Graphical representation of the Tension of domain walls σ_d for different values of k and r. The parameters are fixed at $l = 15.1$, $\lambda = 1.011$, $\eta = 8.9$, $\zeta = 1.9$, $\beta = 2.5$, $H_0 = 71$ and $\gamma = 1$.

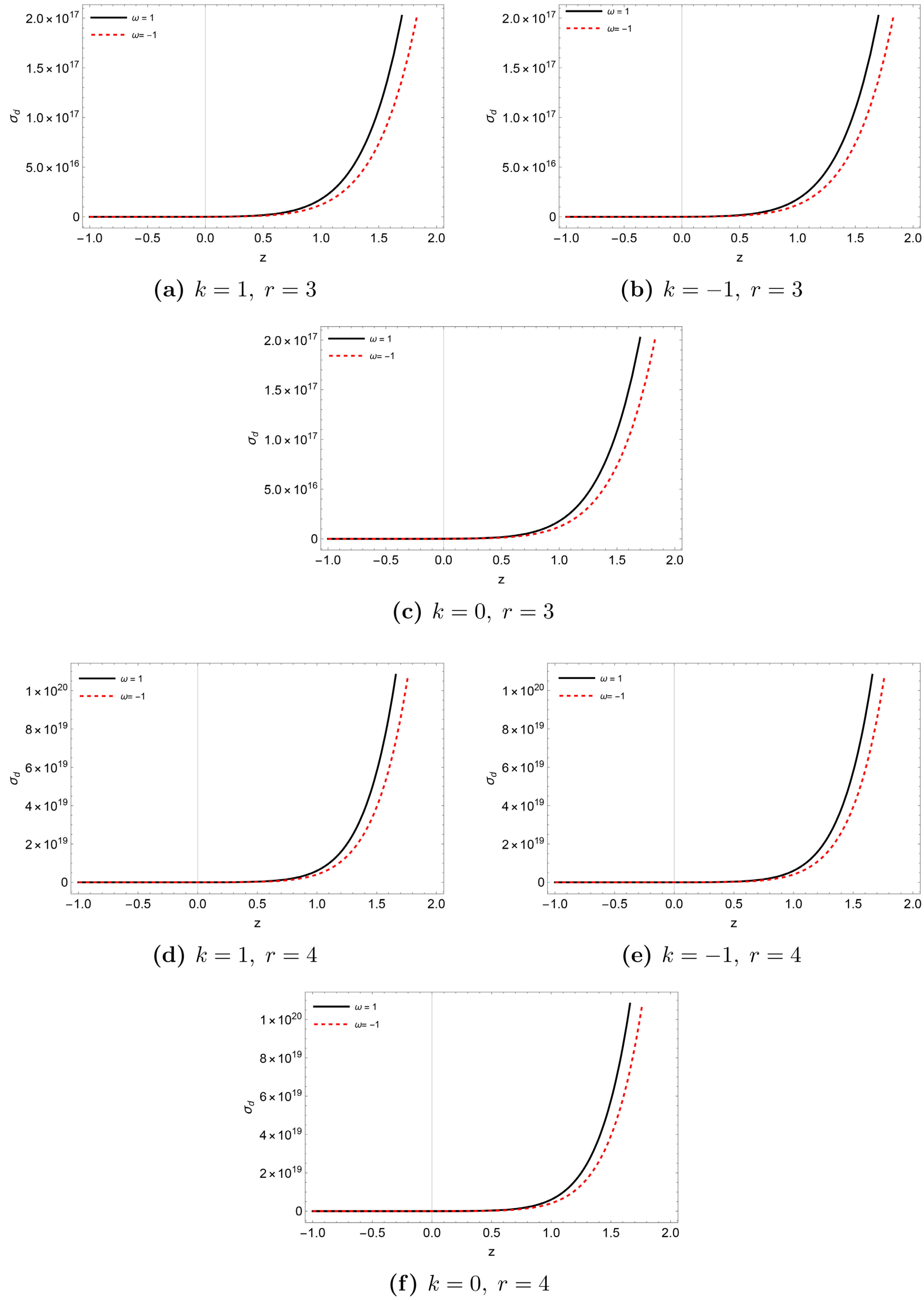

(a) $k = 1,\ r = 3$ **(b)** $k = -1,\ r = 3$

(c) $k = 0,\ r = 3$

(d) $k = 1,\ r = 4$ **(e)** $k = -1,\ r = 4$

(f) $k = 0,\ r = 4$

Figure 9. Graphical representation of the Tension of domain walls σ_d for different values of k and r. The parameters are fixed at $l = 15.1$, $\lambda = 1.011$, $\eta = 8.9$, $\zeta = 1.9$, $\beta = 2.5$, $H_0 = 71$ and $\gamma = 1$.

5. Conclusions

In this paper, we have studied the evolution of Friedmann-Robertson-walker (FRW) space time with domain walls in the framework of $f(R, L_m, T)$ theory of gravitation. We have solved field equations by using deceleration parameter, $p_{eff} = \omega \rho_{eff}$ and two models of $f(R, L_m, T)$ theory. At early time of the universe deceleration parameter is positive and at late time of the universe deceleration parameter is negative. Trajectory of decelerating parameter increases as value of parameter r increases. In model I, at early time of the universe energy density is high and at late time of the universe energy density is decreases and tends to zero. At early time of the universe domain walls is high and positive and at late time of the universe domain walls is decreases and negative.

In model II, at early time of the universe energy density is high and at late time of the universe energy density is decreases and tends to zero. At early time of the universe domain walls is positive and high and at late time of the universe domain walls is decreases and tends to zero. In both model I and model II energy density and domain walls is increases as increasing the parameter r. Change of trajectory of energy density and domain walls is minor for different values of curvature parameter k.

Author Contributions

All authors have same contribution for preparing this manuscript.

Conflicts of Interest

The authors declare no conflicts of interest regarding the publication of this paper.

References

[1] Riess, A.G., Filippenko, A.V., Challis, P., Clocchiatti, A., Diercks, A., Garnavich, P.M., *et al.* (1998) Observational Evidence from Supernovae for an Accelerating Universe and a Cosmological Constant. *The Astronomical Journal*, **116**, 1009-1038. https://doi.org/10.1086/300499

[2] Perlmutter, S., Aldering, G., Goldhaber, G., Knop, R.A., Nugent, P., Castro, P.G., *et al.* (1999) Measurements of ω and λ from 42 High-Redshift Supernovae. *The Astrophysical Journal*, **517**, 565-586. https://doi.org/10.1086/307221

[3] Aghanim, N., *et al.* (2020) Planck 2018 Results. VI. Cosmological Parameters. *Astronomy & Astrophysics*, **641**, A6.

[4] Tegmark, M., Strauss, M.A., Blanton, M.R., Abazajian, K., Dodelson, S., *et al.* (2004) Cosmological Parameters from SDSS and WMAP. *Physical Review D*, **69**, Article ID: 103501.

[5] Carroll, S.M., Press, W.H. and Turner, E.L. (1992) The Cosmological Constant. *Annual Review of Astronomy and Astrophysics*, **30**, 499-542. https://doi.org/10.1146/annurev.aa.30.090192.002435

[6] Einstein, A. (1986) Cosmological Considerations on the General Theory of Relativity. In: Bernstein, J. and Feinberg, G., Eds., *Cosmological Constants: Papers in Modern Cosmology*, Columbia University Press, 16-26.

[7] Peebles, P.J.E. and Ratra, B. (2003) The Cosmological Constant and Dark Energy. *Reviews of Modern Physics*, **75**, 559-606. https://doi.org/10.1103/revmodphys.75.559

[8] Weinberg, S. (1989) The Cosmological Constant Problem. *Reviews of Modern Physics*, **61**, 1-23. https://doi.org/10.1103/revmodphys.61.1

[9] Bull, P., Akrami, Y., Adamek, J., Baker, T., Bellini, E., Beltrán Jiménez, J., *et al.* (2016) Beyond ΛCDM: Problems, Solutions, and the Road Ahead. *Physics of the Dark Universe*, **12**, 56-99. https://doi.org/10.1016/j.dark.2016.02.001

[10] Copeland, E.J., Sami, M. and Tsujikawa, S. (2006) Dynamics of Dark Energy. *International Journal of Modern Physics D*, **15**, 1753-1935. https://doi.org/10.1142/s021827180600942x

[11] Clifton, T., Ferreira, P.G., Padilla, A. and Skordis, C. (2012) Modified Gravity and Cosmology. *Physics Reports*, **513**, 1-189. https://doi.org/10.1016/j.physrep.2012.01.001

[12] Pavón, D. and Radicella, N. (2013) Does the Entropy of the Universe Tend to a Maximum? *General Relativity and Gravitation*, **45**, 63-68. https://doi.org/10.1007/s10714-012-1457-x

[13] Visser, M. (2004) Jerk, Snap and the Cosmological Equation of State. *Classical and Quantum Gravity*, **21**, 2603-2615. https://doi.org/10.1088/0264-9381/21/11/006

[14] Zhang, X. (2005) Statefinder Diagnostic for Holographic Dark Energy Model. *International Journal of Modern Physics D*, **14**, 1597-1606. https://doi.org/10.1142/s0218271805007243

[15] Nojiri, S. and Odintsov, S.D. (2007) Introduction to Modified Gravity and Gravitational Alternative for Dark Energy. *International Journal of Geometric Methods in Modern Physics*, **4**, 115-145. https://doi.org/10.1142/s0219887807001928

[16] Wong, B. (2017) Turaev Torsion Invariants of 3-Orbifolds. *Geometriae Dedicata*, **187**, 179-197. https://doi.org/10.1007/s10711-016-0196-7

[17] Sotiriou, T.P. and Faraoni, V. (2010) f(r) Theories of Gravity. *Reviews of Modern Physics*, **82**, 451-497. https://doi.org/10.1103/revmodphys.82.451

[18] Harko, T., Lobo, F.S.N., Nojiri, S. and Odintsov, S.D. (2011) $f(r,t)$ Gravity. *Physical Review D*, **84**, Article ID: 024020. https://doi.org/10.1103/physrevd.84.024020

[19] Harko, T. and Lobo, F.S.N. (2010) $f(r,l_m)$ Gravity. *The European Physical Journal C*, **70**, 373-379. https://doi.org/10.1140/epjc/s10052-010-1467-3

[20] Harko, T., Koivisto, T.S., Lobo, F.S.N. and Olmo, G.J. (2012) Metric-Palatini Gravity Unifying Local Constraints and Late-Time Cosmic Acceleration. *Physical Review D*, **85**, Article ID: 084016. https://doi.org/10.1103/physrevd.85.084016

[21] Haghani, Z. and Harko, T. (2021) Generalizing the Coupling between Geometry and Matter: $f(r,l_m,t)$ Gravity. *The European Physical Journal C*, **81**, Article No. 615. https://doi.org/10.1140/epjc/s10052-021-09359-3

[22] Zubair, M., Sohail, H., Waheed, S., Ilyas, A. and Mahmood, I. (2026) Stellar Configurations in $f(r,l_m,t)$ Gravity: Probing Anisotropy and Stability via Minimal Geometric Deformation. *Chinese Physics C*, **50**, Article ID: 025103. https://doi.org/10.1088/1674-1137/ae1202

[23] Koussour, M., Altaibayeva, A., Bekova, G., Muminov, S., Davletov, I. and Rayimbaev, J. (2026) Late-Time Acceleration in Extended and Unified $f(r,l_m,t)$ Gravity with Observational Data. *International Journal of Geometric Methods in Modern Physics*, **23**, Article ID: 2550288. https://doi.org/10.1142/s0219887825502883

[24] Kiroriwal, S., Maurya, S.K. and Kumar, J. (2026) Wormholes Generated by a Density-Gradient Dependent Equation of State in $f(r, l_m, t)$ Gravity. *Physics Letters B*, **879**, Article ID: 140639. https://doi.org/10.1016/j.physletb.2026.140639

[25] Naseer, T., Sharif, M., Javed, F., Alrebdi, H.I. and Abdel-Aty, A. (2025) Cosmology in $f(r, l_m, t)$ Gravity Theory Using Gravitational Decoupling. *High Energy Density Physics*, **56**, Article ID: 101217. https://doi.org/10.1016/j.hedp.2025.101217

[26] Mishra, B., Priyobarta, N., *et al.* (2025) Comparative Study on Neutron Star Structure in Linear and Non-Linear Matter-Curvature Coupling in $f(r, l_m, t)$ Gravity Using Equation of States. https://papers.ssrn.com/sol3/papers.cfm?abstract_id=5604773

[27] Moraes, P.H.R.S., Agrawal, A.S. and Mishra, B. (2024) Wormholes in the $f(r, l, t)$ Theory of Gravity. *Physics Letters B*, **855**, Article ID: 138818. https://doi.org/10.1016/j.physletb.2024.138818

[28] Loewer, N., Tayde, M. and Sahoo, P.K. (2024) A Study of Stable Wormhole Solution with Non-Commutative Geometry in the Framework of Linear $f(r, l_m, t)$ Gravity. *The European Physical Journal C*, **84**, Article No. 1196. https://doi.org/10.1140/epjc/s10052-024-13604-w

[29] Katore, S.D., Hatkar, S.P. and Baxi, R.J. (2016) Domain Wall Cosmological Models with Deceleration Parameter in Modified Theory of Gravitation. *Chinese Journal of Physics*, **54**, 563-573. https://doi.org/10.1016/j.cjph.2016.05.005

[30] Katore, S.D. and Hatkar, S.P. (2016) Bianchi Type III and Kantowski-Sachs Domain Wall Cosmological Models in the $f(r, t)$ Theory of Gravitation. *Progress of Theoretical and Experimental Physics*, **2016**, 033E01. https://doi.org/10.1093/ptep/ptw009

[31] Katore, S.D. and Hatkar, S.P. (2015) Strange Quark Matter Coupled to String Cloud in Lyra Geometry. *Astrophysics and Space Science*, **357**, Article No. 55. https://doi.org/10.1007/s10509-015-2265-z

[32] Vilenkin, A. (1981) Gravitational Field of Vacuum Domain Walls and Strings. *Physical Review D*, **23**, 852-857. https://doi.org/10.1103/physrevd.23.852

[33] Ipser, J. and Sikivie, P. (1984) Gravitationally Repulsive Domain Wall. *Physical Review D*, **30**, 712-719. https://doi.org/10.1103/physrevd.30.712

[34] Reddy, D.R.K., Govinda Rao, P. and Naidu, R.L. (2008) Five Dimensional Domain Walls in a Scalar-Tensor Theory of Gravitation. *International Journal of Theoretical Physics*, **47**, 2966-2970. https://doi.org/10.1007/s10773-008-9731-0

[35] Mukherjee, M. (1993) Gravitational Fields of Cosmic Membranes. *Classical and Quantum Gravity*, **10**, 131-146. https://doi.org/10.1088/0264-9381/10/1/014

[36] Pradhan, A., Rai, V. and Otarod, S. (2006) Plane Symmetric Inhomogeneous Bulk Viscous Domain Wall in Lyra Geometry. *Fizika B: A Journal of Experimental and Theoretical Physics*, **15**, 57-70.

[37] Reddy, D.R.K., Naidu, R.L., Dasu Naidu, K. and Ram Prasad, T. (2013) LRS Bianchi Type-II Universe with Cosmic Strings and Bulk Viscosity in a Modified Theory of Gravity. *Astrophysics and Space Science*, **346**, 219-223. https://doi.org/10.1007/s10509-013-1417-2

[38] Saadat, H. (2011) Holographic Dark Energy Density. *International Journal of Theoretical Physics*, **50**, 1769-1775. https://doi.org/10.1007/s10773-011-0685-2

[39] Chaudhary, H., Pacif, S.K.J., Mustafa, G., Atamurotov, F. and Javed, F. (2025) Extracting H_0 and R_d in Q(t) Parametrization Models. *Journal of High Energy Astrophysics*, **45**, 340-349. https://doi.org/10.1016/j.jheap.2025.01.001

[40] Hatkar, S.P., Tadas, D.P. and Katore, S.D. (2024) Domain Wall and Holographic Dark Energy in F(q) Theory of Gravity. *International Journal of Geometric Methods in Modern Physics*, **21**, Article ID: 2440033. https://doi.org/10.1142/s0219887824400334

[41] Chingkheinganba Meetei, E. and Surendra Singh, S. (2026) Phase-Space Structure and Stability Analysis in $f(r, l_m, t)$ Gravity. *Modern Physics Letters A*, **41**, Article ID: 2650122. https://doi.org/10.1142/s0217732326501221